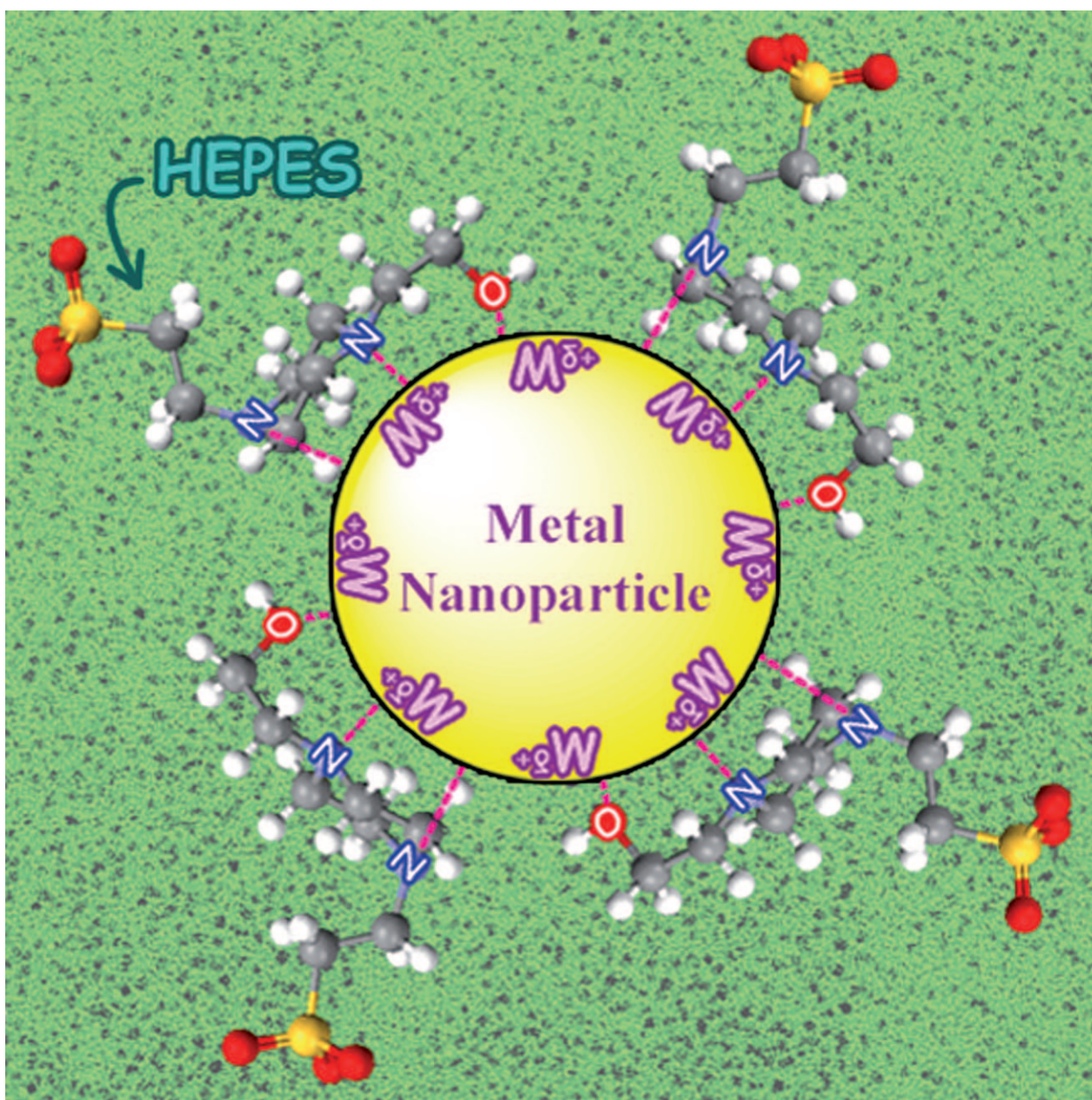


## Hydrothermal Synthesis of Platinum-Group-Metal Nanoparticles by Using HEPES as a Reductant and Stabilizer\*\*

Man-Ho So,<sup>[a]</sup> Chi-Ming Ho,<sup>[a]</sup> Rong Chen,<sup>[b]</sup> and Chi-Ming Che<sup>\*[a]</sup>



**Abstract:** Platinum-group-metal (Ru, Os, Rh, Ir, Pd and Pt) nanoparticles are synthesized in an aqueous buffer solution of 4-(2-hydroxyethyl)-1-piperazineethanesulfonic acid (HEPES) (200 mM, pH 7.4) under hydrothermal conditions (180°C). Monodispersed (monodispersity: 11–15%) metal nanoparticles were obtained with an average particle size of less than 5 nm (Ru:  $1.8 \pm 0.2$ , Os:  $1.6 \pm 0.2$ , Rh:  $4.5 \pm 0.5$ , Ir:  $2.0 \pm 0.3$ , Pd:  $3.8 \pm 0.4$ , Pt:  $1.9 \pm 0.2$  nm).

The size, monodispersity, and stability of the as-obtained metal nanoparticles were affected by the HEPES concentration, pH of the HEPES buffer solution, and reaction temperature. HEPES with two tertiary amines (pi-

perazine groups) and terminal hydroxyl groups can act as a reductant and stabilizer. The HEPES molecules can bind to the surface of metal nanoparticles to prevent metal nanoparticles from aggregation. These platinum-group-metal nanoparticles could be deposited onto the surface of graphite, which catalyzed the aerobic oxidation of alcohols to aldehydes.

**Keywords:** HEPES buffer • hydrothermal synthesis • nanoparticles • platinum-group metals • supported catalysts

## Introduction

The development of new synthetic methods for monodispersed nanomaterials is crucial for their subsequent applications in electronics<sup>[1]</sup> and biological and catalytic sciences.<sup>[2–4]</sup> In particular, platinum-group-metal (Ru, Os, Ir, Rh, Pt, and Pd) nanoparticles have demonstrated superior catalytic activities relative to their bulk counterparts due to their large surface area to volume ratios and the high density of active sites on their surface.<sup>[3]</sup> A well-known method for the synthesis of monodispersed platinum-group-metal nanoparticles is through polyol (alcohol) reduction in the presence of capping agents (e.g. polyvinylpyrrolidone (PVP), polyethylene glycol (PEG), and cetyltrimethylammonium bromide (CTAB)).<sup>[5]</sup> Another method is the decomposition of organometallic precursors to generate metal nanoparticles under carefully controlled conditions.<sup>[5,6]</sup> Although both methods are able to produce metal nanoparticles with a narrow monodispersity and well-defined morphology,<sup>[7]</sup> these methods suffer from the drawbacks of using hazardous organic solvents and chemicals, both of which are undesirable in the context of green chemistry and biological application studies. In this regard, there has been considerable interest in the development of methods for the synthesis of metal nanoparticles in aqueous medium and without the use of toxic reagents. In addition, a reagent playing dual roles as a reductant of metal salts and a stabilizer of metal nanoparticles would be appealing.

Over the past few years, the synthesis of metal nanoparticles in aqueous medium without the generation of hazardous substances has received increasing attention.<sup>[8]</sup> Wallen and co-workers reported the “green” synthesis of Ag, Au, and Au–Ag alloy nanoparticles, involving glucose and starch as both a reductant and stabilizer.<sup>[9]</sup> Xia reported a general synthesis of noble metal (Pd, Pt, Ag, and Au) nanoplates by using PVP to act as both a reductant and stabilizer.<sup>[10]</sup> Recently, we reported the use of biocompatible 4-(2-hydroxyethyl)-1-piperazineethanesulfonic acid (HEPES) for the synthesis of Ag nanoparticles (average particle size about 10 nm), which was found to display cyto-protective activities towards HIV-1 infected cells.<sup>[2c]</sup> The Ag nanoparticles could also be synthesized by the reduction of  $\text{Ag}^+$  with HEPES and branched polyethyleneimine.<sup>[11]</sup> Branched, flowered or spherical Au nanoparticles could also be synthesized in HEPES buffer solutions at ambient conditions without the addition of surfactants or seeds.<sup>[12]</sup>

We envision that the mild reducing property of HEPES allows the feasibility of controlling the kinetics of the reduction process by varying the reaction temperature or pH of the buffer solution. Herein is described a general synthetic route for both monodispersed (monodispersity: 11–15%) and small sized (<5 nm) platinum-group-metal nanoparticles in HEPES buffer (200 mM, pH 7.4) under hydrothermal conditions. We show that HEPES acts as a reductant and a stabilizer for the formation of metal nanoparticles. The piperazine group of HEPES accounts for the reduction of metal salts and the stabilization of metal nanoparticles. We have also demonstrated that these metal nanoparticles could be deposited onto the surface of graphite, which catalyzes the aerobic oxidation of alcohols to aldehydes.

## Results and Discussion

### Synthesis and characterization of metal nanoparticles

*Screening of buffer systems for nanoparticle synthesis:* Recently, we reported that HEPES can act as both a reductant and a stabilizer for the synthesis of Ag and Au nanoparticles in aqueous solutions.<sup>[2c,12d]</sup> In this work, the use of HEPES

[a] Dr. M.-H. So, Dr. C.-M. Ho, Prof. C.-M. Che  
Department of Chemistry and Open Laboratory  
of Chemical Biology of the Institute of Molecular  
Technology for Drug Discovery and Synthesis  
The University of Hong Kong  
Pokfulam Road, Hong Kong SAR (China)  
Fax: (+852)2857-1586  
E-mail: cmche@hku.hk

[b] Dr. R. Chen  
Key Laboratory for Green Chemical Process of Ministry  
of Education and School of Chemical Engineering & Pharmacy  
Wuhan Institute of Technology  
Xiongchu Street, Wuhan, 430073 (China)

[\*\*] HEPES = 4-(2-hydroxyethyl)-1-piperazineethanesulfonic acid.

Supporting information for this article is available on the WWW  
under <http://dx.doi.org/10.1002/asia.201000066>.

and other biocompatible buffers for the synthesis of metal nanoparticles of platinum-group metals (Ru, Os, Rh, Ir, Pd, and Pt) in aqueous medium has further been explored under hydrothermal conditions. At the outset, the metal salt (2 mM) was first dissolved into an aqueous HEPES buffer solution (200 mM, pH 7.4) in a Teflon-lined stainless-steel autoclave. The reactor was incubated at 180 °C for an hour. Examination of the HEPES buffer before and after the hydrothermal reaction by NMR spectroscopy did not show any significant difference in the spectra, which revealed that the HEPES molecules are stable under hydrothermal conditions (see Figure S1 in the Supporting Information). The reaction was considered to be completed when the UV/Vis absorption spectrum of the reaction mixture did not change further (see Figure S2 in the Supporting Information), and/or diffraction peaks due to the metal salts disappeared in the powder XRD spectrum. All of these metal nanoparticles suspended in water with no apparent aggregation or flocculation of metal nanoparticles for weeks, which revealed that HEPES is a good stabilizer, preventing the metal nanoparticles from aggregation.

Examination of a suspension of metal nanoparticles by transmission electron microscopy (TEM) revealed that spherical metal nanoparticles with uniform sizes were obtained (Figure 1). The average diameters of Ru, Os, Rh, Ir, Pd, and Pt nanoparticles were  $1.8 \pm 0.2$ ,  $1.6 \pm 0.2$ ,  $4.5 \pm 0.5$ ,  $2.0 \pm 0.3$ ,  $3.8 \pm 0.4$ , and  $1.9 \pm 0.2$  nm, respectively (Table 1). The monodispersities of these metal nanoparticles were not more than 15%, indicating that these nanoparticles were monodispersed. When the reaction time was extended to 3 h, serious aggregation of metal nanoparticles was noted. Figure 2 shows a typical TEM image of aggregated Os nanoparticles obtained from the treatment of Os metal salt (2 mM) in HEPES buffer solution (200 mM, pH 7.4) for 3 h and under hydrothermal conditions at 180 °C.

High-resolution transmission electron microscopy (HRTEM) allows the imaging of metal nanoparticles at the atomic level and can be used for the analysis of their crystallographic structures. As depicted in Figure 3, these metal nanoparticles displayed excellent crystallinity as revealed by the clear lattice fringes and sharp diffraction spots in the fast Fourier transform (FFT) images of the interested nano-

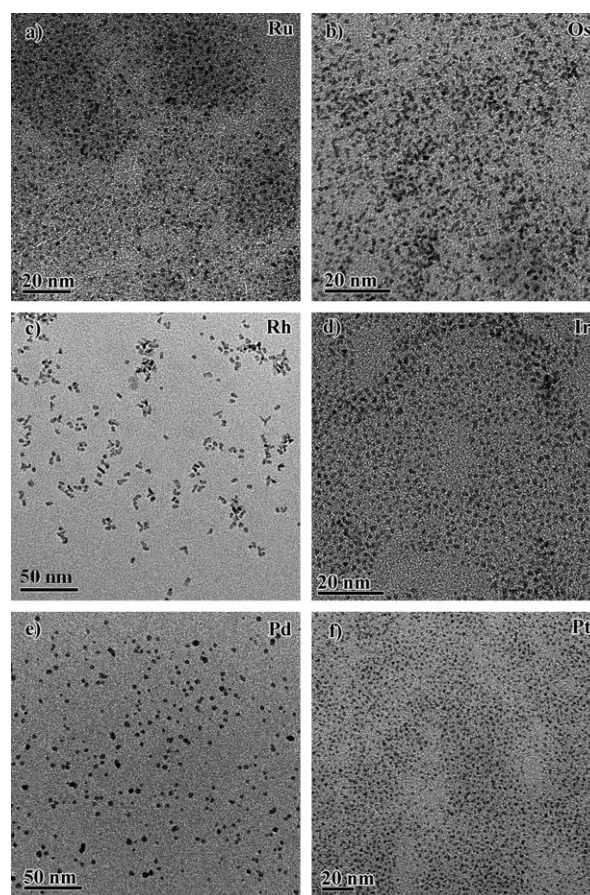


Figure 1. TEM images of a) Ru, b) Os, c) Rh, d) Ir, e) Pd, and f) Pt nanoparticles prepared in HEPES buffer (200 mM, pH 7.4) under hydrothermal conditions at 180 °C for 1 h.

Table 1. Average diameter and monodispersity of the metal nanoparticles prepared in HEPES buffer (200 mM, pH 7.4) under hydrothermal conditions at 180 °C for 1 h.

Metal nanoparticles	$d$ [nm] <sup>[a]</sup>	Monodispersity [%] <sup>[b]</sup>
ruthenium	$1.8 \pm 0.2$	11
osmium	$1.6 \pm 0.2$	13
rhodium	$4.5 \pm 0.5$	11
iridium	$2.0 \pm 0.3$	15
palladium	$3.8 \pm 0.4$	11
platinum	$1.9 \pm 0.2$	11

[a] The average diameter ( $d$ ) is measured from 300 randomly selected nanoparticles. [b] Monodispersity of the diameter of nanoparticles is calculated as follows: monodispersity = (standard deviation/average diameter)  $\times$  100%.

particles (insets in Figure 3). The Rh nanoparticles revealed a twinned crystal structure as shown by the HRTEM image depicted in Figure 3c, whereas the HRTEM images of the other metal (Ru, Os, Ir, Pt, and Pd) nanoparticles showed that they were single crystals. Those lattice spacings ( $d$ -spacing) could be indexed back to the crystal planes of their corresponding bulk metals further confirming the identities of the metal nanoparticles at the microscopic level.

#### Abstract in Traditional Chinese:

在本工作中，我們使用水相 HEPES (200 mM, pH 7.4) 緩衝溶液，在熱液條件下 (180 °C) 合成了鉑系金屬 (鈦，鉻，鈦，鈷，鈀和鉑) 納米顆粒。反應後，得到尺寸小於 5 納米單分散的 (單分散性: 11–15%) 金屬納米顆粒 (鈦:  $1.8 \pm 0.2$  nm; 鉻:  $1.6 \pm 0.2$  nm; 鈦:  $4.5 \pm 0.5$  nm; 鈷:  $2.0 \pm 0.3$  nm; 鈀:  $3.8 \pm 0.4$  nm; 鉑:  $1.9 \pm 0.2$  nm)。納米顆粒的尺寸，單分散性和穩定性由 HEPES 緩衝溶液的濃度，pH 值和反應溫度控制。緩衝劑 HEPES 分子中的兩個三級胺基團 (咪嗪基團) 和一個末端醇羥基可以用作還原劑和穩定劑。HEPES 分子可以覆蓋在金屬納米顆粒的表面，阻止其進一步聚合。將這些鉑系金屬納米顆粒負載於石墨，可用於催化醇類化合物的耗氣氧化成醛類化合物。

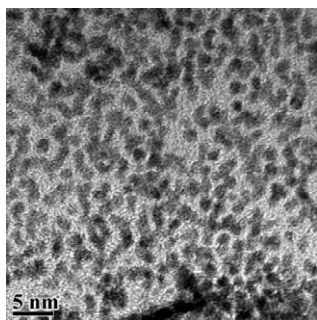


Figure 2. TEM images of the Os nanoparticles prepared in HEPES buffer (200 mM, pH 7.4) under hydrothermal conditions at 180 °C for 3 h.

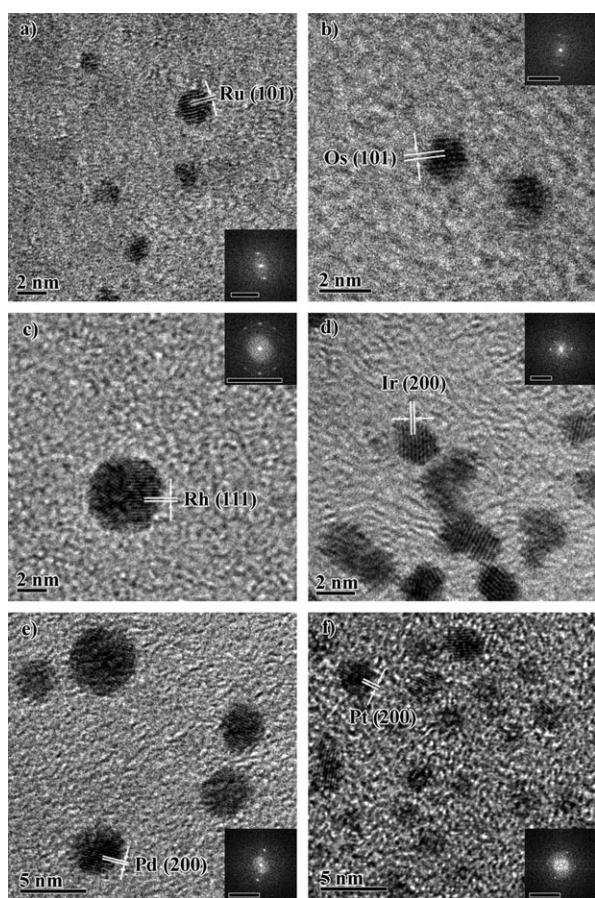


Figure 3. HRTEM images of a) Ru, b) Os, c) Rh, d) Ir, e) Pd, and f) Pt nanoparticles prepared in HEPES buffer (200 mM, pH 7.4) under hydrothermal conditions at 180 °C for 1 h. Insets are the FFT images of the interesting nanoparticles. The scale bars in the insets are 10 nm<sup>-1</sup>.

Energy dispersive X-ray (EDX) analysis was performed to examine the elemental compositions of the metal nanoparticles (see Figure S3 in the Supporting Information). Each EDX spectrum of nanoparticles reveals the presence of the corresponding metal. The presence of both Cu and C are attributed to the Formvar-coated copper grids. The HEPES accounts for the presence of C, O, and S.

**Powder X-ray diffraction (XRD) analysis:** Dry solid samples have also been characterized by powder XRD for examining the composition(s) and/or identity of the products. To improve the crystallinity of the samples for better resolution of the diffraction peaks, calcination (550 °C, 6 h and argon atmosphere) was applied on some of the samples. As depicted in Figure 4, all of the solid samples showed a diffraction pattern that matches to the standard metal patterns (JCPDS file of Ru: 06-0663, Os: 06-0662, Rh: 05-0685, Ir: 06-0598, Pd: 46-1043, Pt: 04-0802). Broadening of the diffraction peaks of the metal nanoparticles is attributed to the small crystal size of the nanoparticles and we have calculated the average particle size by using the Scherrer equation as tabulated in Table S1 in the Supporting Information.<sup>[13]</sup>

**X-ray photoelectron spectroscopy (XPS) analysis:** We have examined the surface chemical oxidation state of the metal nanoparticles by XPS analysis. As depicted in Table 2, all of the binding energies of the interested peaks could be assigned to the corresponding metal by comparison with literature values.<sup>[14]</sup> The binding energy of the 3p<sub>3/2</sub> peak of the Ru nanoparticles obtained in this work is 462.7 eV, which is slightly higher than the literature value (462.0 eV).<sup>[3h,14]</sup> This reveals that the surface of the Ru nanoparticles contained oxidized Ru species.

**Role of HEPES buffer:** HEPES contains three functional groups: a sulfonic acid group, a piperazine group, and a terminal hydroxyl group. To gain an insight into the role of these groups, we examined three other zwitterionic N-substituted aminosulfonic acid buffers (3-[4-(2-hydroxyethyl)-1-piperazinyl]propanesulfonic acid (EPPS), piperazine-*N,N'*-bis(2-ethanesulfonic acid) (PIPES), and 2-(*N*-morpholino)ethanesulfonic acid (MES)). As an example, Ir nanoparticles

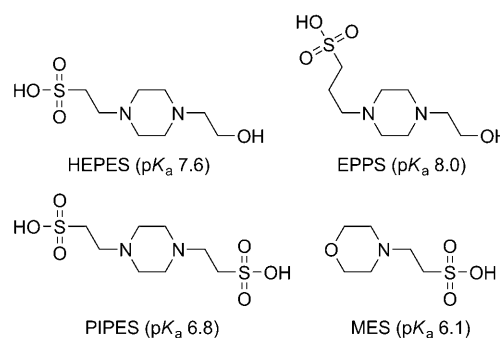


Table 2. Binding energy values of the metal nanoparticles at 3p<sub>3/2</sub> (Ru), 3d<sub>5/2</sub> (Rh and Pd), or 4f<sub>7/2</sub> (Os, Ir, and Pt).

Metal nanoparticles <sup>[a]</sup>	Binding energy [eV] <sup>[b]</sup>	Assignment
ruthenium (3p <sub>3/2</sub> )	462.7 (462.0)	Ru(0)
osmium (4f <sub>7/2</sub> )	51.0 (50.7)	Os(0)
rhodium (3d <sub>5/2</sub> )	307.3 (307.2)	Rh(0)
iridium (4f <sub>7/2</sub> )	61.0 (60.9)	Ir(0)
palladium (3d <sub>5/2</sub> )	335.3 (335.1)	Pd(0)
platinum (4f <sub>7/2</sub> )	71.0 (71.2)	Pt(0)

[a] Corresponding peak for XPS analysis is shown in parentheses.  
 [b] Standard binding energy values are shown in parentheses.

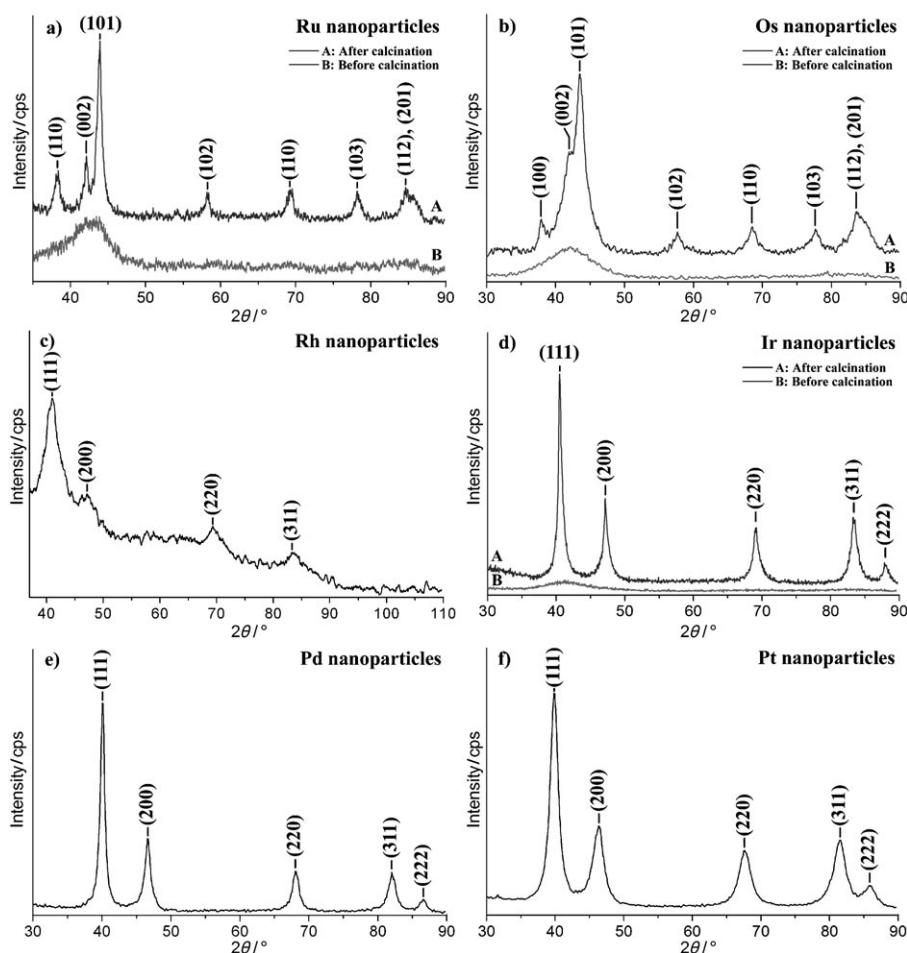


Figure 4. Powder XRD pattern of a) Ru, b) Os, c) Rh, d) Ir, e) Pd, and f) Pt nanoparticles. Plots A and B are the XRD pattern of the nanoparticles after calcination at 550°C for 6 h under an argon atmosphere and before calcination, respectively.

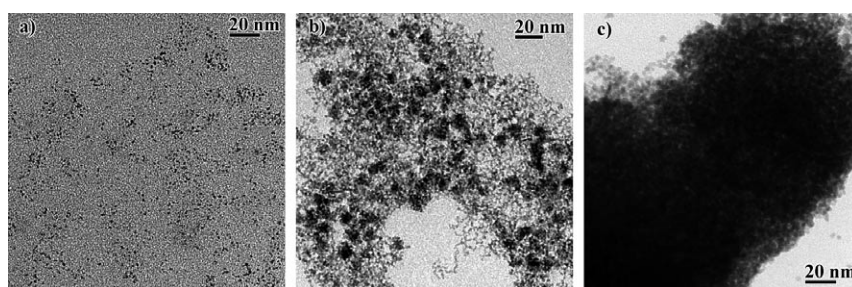


Figure 5. TEM images of the Ir nanoparticles prepared in a) EPPS (200 mM, pH 8.0), b) PIPES (200 mM, pH 6.8), and c) MES buffer (200 mM, pH 6.4) under hydrothermal conditions at 180°C for 1 h.

were prepared by using aqueous buffer solutions of EPPS, PIPES, and MES individually under hydrothermal conditions at 180°C for one hour. No significant difference in sizes and shapes of the Ir nanoparticles were noted when EPPS buffer was used (Figure 5a). The average particle size and monodispersity of the Ir nanoparticles were  $2.1 \pm 0.3$  nm and 12.1%, respectively. When PIPES or MES buffer was used, reduction of Ir salts took place but the Ir nanoparticles

were seriously aggregated (Figure 5b–c). This result indicates that the tertiary amine in either the piperazine (HEPES, EPPS, and PIPES) or morpholine group (MES) is capable of reducing the metal salts. The terminal hydroxyl group in HEPES or EPPS might also act as reductant. Importantly, the terminal hydroxyl group is crucial to the stabilization of metal nanoparticles as illustrated by serious aggregation of metal nanoparticles in PIPES and MES buffer (cf. Figure 1d with 5b–c).

Next, we examined the effect of pH (5.4–9.4) on the formation of metal nanoparticles. In the case of Ir nanoparticles, its stability is sensitive to the pH of the reaction medium (Figure 6). The Ir nanoparticles in this work were found to seriously aggregate at pH 5.4. Little aggregation was noted for the Ir nanoparticles prepared at pH 6.4. Well-dispersed Ir nanoparticles could be successfully obtained at pH 7.4–9.4. There is no significant change in the average particle size of Ir nanoparticles by altering the pH of the reaction medium (Table 3). At pH 5.4, the predominant form of HEPES is a singly protonated amine. When the pH of the buffer increases, the concentration of the deprotonated form of HEPES increases. We propose that the two free nitrogen atoms (piperazine group) in the deprotonated form of HEPES bind to the surface of the metal nanoparticles, thereby prohibiting the metal nanoparticles from aggregation.

The HEPES concentration is another factor affecting the stability of metal nanoparticles. As mentioned before, all metal nanoparticles prepared in HEPES buffer (pH 7.4) at 200 mM under hydrothermal conditions at 180°C were stable without aggregation. When the concentration of HEPES was lowered to 50 mM, only Os and Ir nanoparticles with a good stability were found, whereas Pt nanoparticles were found to aggregate and precipitate at the bottom of the reaction vessel (Figure 7).

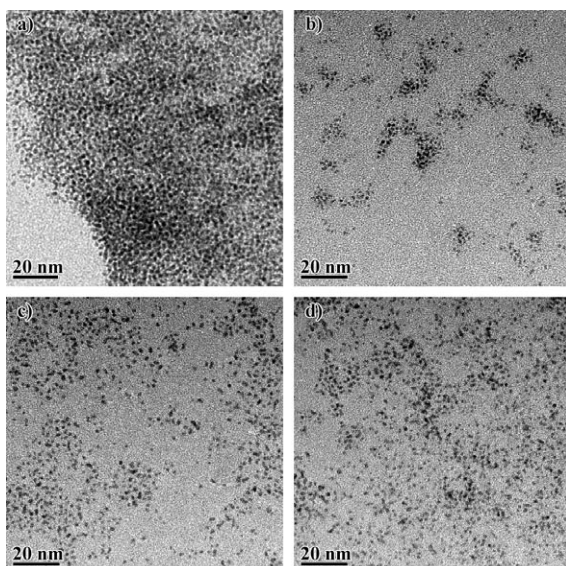


Figure 6. TEM images of the Ir nanoparticles prepared in HEPES solution (200 mM) of pH a) 5.4, b) 6.4, c) 8.4, and d) 9.4 under hydrothermal conditions at 180 °C for 1 h.

Table 3. Average diameter and monodispersity of the Ir nanoparticles prepared in HEPES buffer (200 mM) under hydrothermal conditions at 180 °C for 1 h at various pH values.

pH	$d$ [nm] <sup>[a]</sup>	Monodispersity [%] <sup>[b]</sup>
5.4	$2.2 \pm 0.3$	14
6.4	$1.9 \pm 0.3$	16
7.4	$2.0 \pm 0.3$	15
8.4	$2.0 \pm 0.2$	10
9.4	$2.0 \pm 0.2$	10

[a] The average diameter ( $d$ ) is measured from 300 randomly selected nanoparticles. [b] Monodispersity of the diameter of nanoparticles is calculated as follows: monodispersity = (standard deviation/average diameter)  $\times$  100 %.

TEM analysis revealed that the Os and Ir nanoparticles were approximately spherical in shape with an average size of 2.3 and 2.2 nm, respectively. However, Pt nanoparticles were aggregated and the particle size was about 3.1 nm (Figure 7). Heavy precipitation was found for all of the preparations conducted at an even lower concentration of

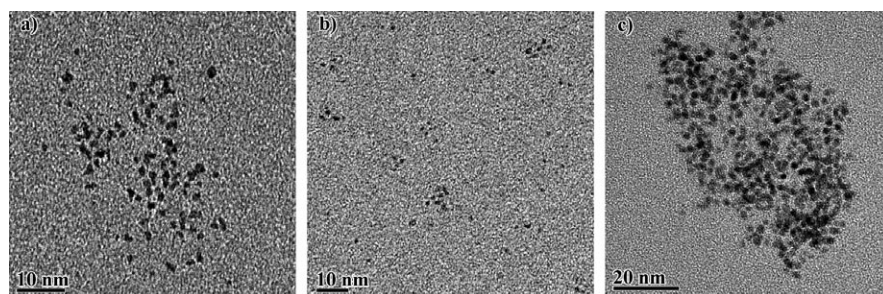


Figure 7. TEM images of the a) Os, b) Ir, and c) Pt nanoparticles prepared in HEPES buffer (50 mM, pH 7.4) under hydrothermal conditions at 180 °C for 1 h.

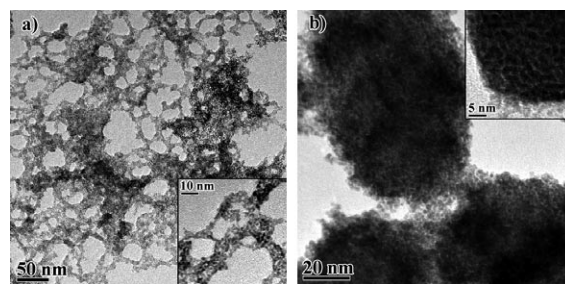


Figure 8. TEM images of a) Os and b) Ir nanoparticles prepared in HEPES buffer (5 mM, pH 7.4) under hydrothermal conditions at 180 °C for 1 h. Insets are the TEM images of the same samples at higher resolution.

HEPES (5 mM; pH 7.4) (TEM images of Os and Ir nanoparticles are depicted in Figure 8 as examples).

*Effect of reaction temperature:* The effect of reaction temperature on the synthesis of metal nanoparticles has been examined. As an example, well-dispersed Ru nanoparticles could be obtained at 140 °C. However, when the reaction temperature was increased to 220 °C, a metallic black powder containing seriously aggregated Ru nanoparticles was found in the reaction vessel (Figure 9).

The synthesis of metal nanoparticles by refluxing the reaction mixture under atmospheric conditions has also been examined. No reduction of Rh salts was noted after refluxing Rh salts in HEPES solution (200 mM, pH 7.4) for one hour.

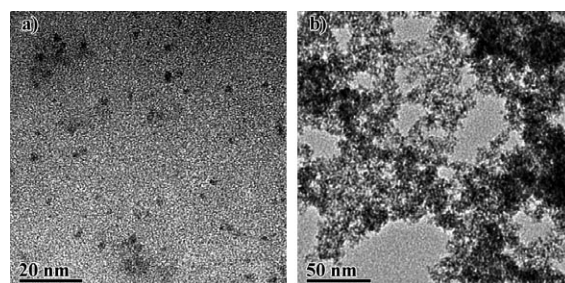


Figure 9. TEM images of the Ru nanoparticles prepared in HEPES buffer (200 mM, pH 7.4) under hydrothermal conditions at a) 140 and b) 220 °C for 1 h.

In the case of Ru, Os, or Ir, a black precipitate of aggregated metal nanoparticles was obtained (TEM images of Os and Ir nanoparticles are shown as examples; Figure 10). Well-segregated Pt and Pd nanoparticles could be prepared under reflux conditions as revealed by TEM images (Figure 10). The particle sizes of Pt and Pd nanoparticles were  $2.9 \pm 0.3$  and  $5.1 \pm 0.8$  nm,

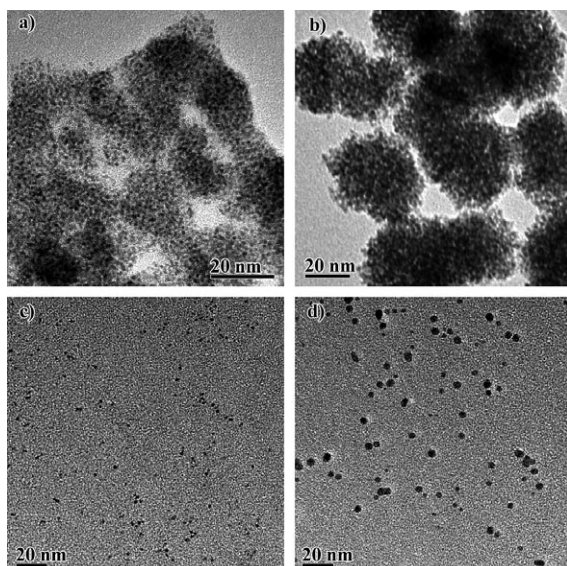


Figure 10. TEM images of the a) Os, b) Ir, c) Pt, and d) Pd nanoparticles prepared in HEPES solution (200 mM, pH 7.4) under reflux at 100 °C for 1 h.

respectively. It should be noted that the sizes of Pt and Pd nanoparticles prepared under reflux conditions were significantly larger than those prepared by the hydrothermal process. The hydrothermal process provides an elevated reaction temperature and pressure, which may probably increase the reactivity of HEPES towards the reduction of metal salts.<sup>[5a]</sup> The increased reactivity of HEPES results in a fast nucleation step, thus the metal nanoparticles obtained by the hydrothermal process are usually smaller and more uniform in size.

**Graphite-supported platinum-group-metal nanoparticles:** One potential application of metal nanoparticles is in the catalysis area.<sup>[3]</sup> Metal nanoparticles are usually deposited onto the surface of the solid support, taking the advantage of the easy separation of these solid supported catalysts from reaction mixture. The solid support could affect the electronic properties of nanoparticles (e.g. gold nanoparticles supported on cerium(IV) oxide).<sup>[15]</sup>

In this work, the graphite-supported metal nanoparticles (MNPs/C) catalysts were prepared by deposition of the freshly prepared metal nanoparticles onto the surface of graphite at a metal loading of 0.1 mmol g<sup>-1</sup>. As revealed by the TEM images of the MNPs/C catalysts, these nanoparticles were deposited onto the surface of graphite without serious aggregation (Figure 11). The average particle sizes of Ru, Os, Rh, Ir, Pd, and Pt nanoparticles were 2.1 ± 0.2, 2.0 ± 0.2, 4.6 ± 0.6, 2.1 ± 0.2, 11.8 ± 1.3, and 3.0 ± 0.3 nm, respectively. The size of the Rh and Ir nanoparticles did not significantly change, whereas the sizes of the Ru, Os, Pd, and Pt nanoparticles increased after grafting onto the surface of graphite. An increase in the size of the nanoparticles after deposition onto the surface of graphite has previously been reported<sup>[3]</sup> and the mechanism for the enlargement of nanoparticles after deposition onto graphite is under investiga-

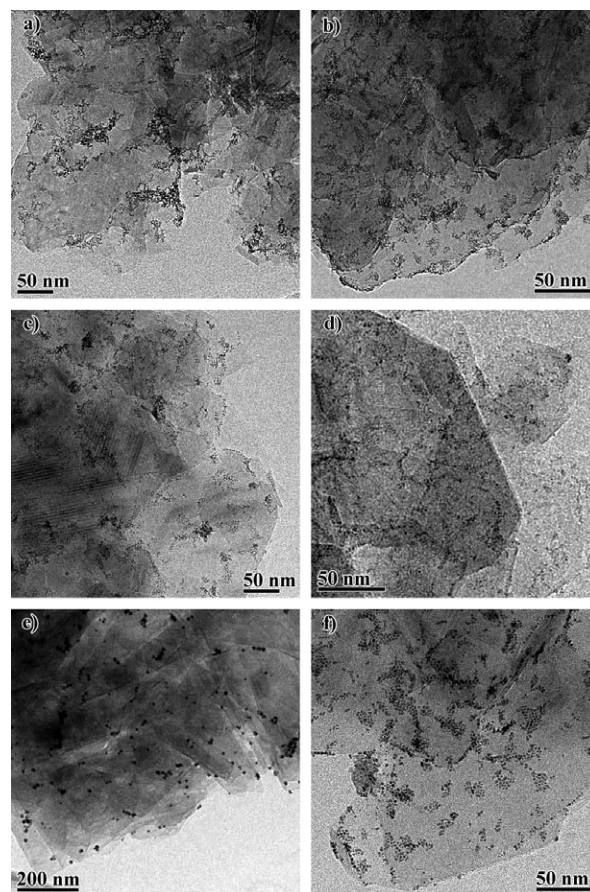
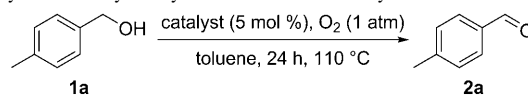


Figure 11. TEM images of the graphite-supported a) Ru, b) Os, c) Rh, d) Ir, e) Pd, and f) Pt nanoparticle catalysts.

tion. These metal nanoparticles maintained their uniformity after deposition onto the surface of graphite (monodispersity of Ru nanoparticles: 9.5, Os: 10.0, Rh: 13.0, Ir: 9.5, Pd: 11.0, Pt: 10.0 %).

We further examined the catalytic activities of these MNPs/C catalysts towards the aerobic oxidation of alcohols.<sup>[15,16]</sup> As depicted in Table 4, OsNPs/C can catalyze the

Table 4. Aerobic oxidation of 4-methylbenzyl alcohol **1a** to 4-methylbenzaldehyde **2a** catalyzed by various MNPs/C catalysts.<sup>[a]</sup>

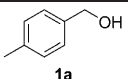
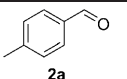
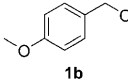
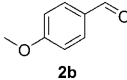
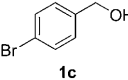
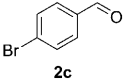
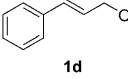
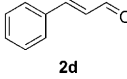
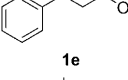
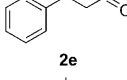
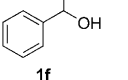
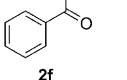


Entry	Catalyst	Conv. [%] <sup>[b]</sup>	Yield [%] <sup>[b,c]</sup>
1	RuNPs/C	89	90
2	OsNPs/C	92	93
3	RhNPs/C	10	70
4	IrNPs/C	38	73
5	PdNPs/C	<5	65
6	PtNPs/C	<5	68
7 <sup>[d]</sup>	graphite	0	0

[a] Reaction conditions: **1a** (0.4 mmol), MNPs/C (metal: 5 mol %), toluene (5 mL), O<sub>2</sub> (1 atm.), 110 °C, 24 h, unless otherwise stated. [b] Conversion and yield were determined by <sup>1</sup>H NMR spectroscopy by using Ph<sub>2</sub>C=CH<sub>2</sub> as the internal standard. [c] The yield was calculated based on substrate conversion. [d] Graphite (200 mg) was used.

aerobic oxidation of alcohol **1a** with excellent substrate conversion and product yield (Table 4, entry 2). By using the “OsNPs/C+O<sub>2</sub>” protocol, other primary and secondary alcohols can also be effectively oxidized into aldehydes and ketones, respectively, with product yields of up to 93 % (Table 5).

Table 5. Aerobic oxidation of alcohol **1** by using the “OsNPs/C+O<sub>2</sub>” protocol.<sup>[a]</sup>

$\begin{array}{c} \text{R}^2/\text{H} \\   \\ \text{R}-\text{C}-\text{OH} \\   \\ \text{1} \end{array} \xrightarrow[\text{O}_2 (1 \text{ atm}), \text{ toluene}, 110^\circ \text{C}]{\text{OsNPs/C (Os: 5 mol \%)}} \begin{array}{c} \text{R}^2/\text{H} \\   \\ \text{R}-\text{C}=\text{O} \\   \\ \text{2} \end{array}$					
Entry	Substrate	Product	<i>t</i> [d]	Conv. [%] <sup>[b]</sup>	Yield [%] <sup>[b,c]</sup>
1			1.5	100	93
2			1.5	100	75 <sup>[d]</sup>
3			2	100	93
4			2	87	80
5			2	44	58
6			4	81	41

[a] Reaction conditions: **1** (0.4 mmol), OsNPs/C (Os: 5 mol %), toluene (5 mL), O<sub>2</sub> (1 atm.), 110 °C, 24 h, unless otherwise stated. [b] Conversion and yield were determined by <sup>1</sup>H NMR spectroscopy by using Ph<sub>2</sub>C=CH<sub>2</sub> as the internal standard. [c] Yield was calculated based on substrate conversion. [d] A 15 % yield of *p*-anisic acid was found.

We have also examined the reactions of first-row d-block transition-metal salts in HEPES buffer solution under hydrothermal conditions. Metal oxide nanocrystals (Mn<sub>3</sub>O<sub>4</sub> nanooctahedrons, Co<sub>3</sub>O<sub>4</sub> nanocubes, and ZnO nanorods) were obtained when their corresponding metal salts (MnSO<sub>4</sub>·4H<sub>2</sub>O, CoCl<sub>2</sub>·6H<sub>2</sub>O, or ZnCl<sub>2</sub>) were used under hydro-

thermal conditions in HEPES buffer solution (200 mM, pH 7.4). No zero-valent metal nanoparticles were obtained probably due to the large negative reduction potentials for the reduction of these metal salts to elemental metal in the zero oxidation state.<sup>[10]</sup> TEM images of the Mn<sub>3</sub>O<sub>4</sub> nanooctahedrons, Co<sub>3</sub>O<sub>4</sub> nanocubes, and ZnO nanorods are depicted in Figure 12 and the details of characterization are given in Part IV of the Supporting Information.

## Conclusions

We have demonstrated the synthesis of a variety of platinum-group-metal nanoparticles (Ru, Os, Rh, Ir, Pt, and Pd) and metal oxide nanocrystals (Mn<sub>3</sub>O<sub>4</sub> nanooctahedrons, Co<sub>3</sub>O<sub>4</sub> nanocubes, and ZnO nanorods) by one-pot hydrothermal reactions in aqueous HEPES buffer solutions (200 mM, pH 7.4). All these platinum-group-metal nanoparticles are spherical and monodispersed with a size of less than 5 nm (Ru: 1.8 ± 0.2, Os: 1.6 ± 0.2, Rh: 4.5 ± 0.5, Ir: 2.0 ± 0.3, Pd: 3.8 ± 0.4, Pt: 1.9 ± 0.2 nm). These metal nanoparticles were found to exhibit excellent crystallinity as confirmed by their HRTEM images. Based on the comparison with other buffer solutions (EPPS, PIPES, and MES) and the study on the effect of metal salt concentration and pH of HEPES buffer, we propose that HEPES functions as both a reductant and a stabilizer. The elevated temperature and pressure provided by hydrothermal conditions are crucial to increase the reactivity of HEPES towards the reduction of metal salts. Moreover, these metal nanoparticles can be deposited onto the surface of graphite and act as potential heterogeneous catalysts for organic transformation reactions (e.g. aerobic oxidation of alcohols to aldehydes). Considering its simplicity and the use of biocompatible HEPES buffer, this synthetic protocol could be used to produce biocompatible metal nanoparticles for biological studies.

## Experimental Section

**Chemicals:** All the chemicals (analytical reagent grade) were purchased from Aldrich and used as received without further purification unless otherwise noted. HEPES, EPPS, PIPES, MES, manganese(II) sulfate tetrahydrate (MnSO<sub>4</sub>·4H<sub>2</sub>O), cobalt(II) chloride (CoCl<sub>2</sub>·6H<sub>2</sub>O), and zinc(II) chloride (ZnCl<sub>2</sub>) were purchased from Aldrich. Ruthenium(III) chloride hydrate (RuCl<sub>3</sub>·xH<sub>2</sub>O), rhodium(III) chloride hydrate (RhCl<sub>3</sub>·xH<sub>2</sub>O), iridium(III) chloride hydrate (IrCl<sub>3</sub>·xH<sub>2</sub>O), palladium(II) chloride (PdCl<sub>2</sub>), and potassium tetrachloroplatinate(II) (K<sub>2</sub>[PtCl<sub>4</sub>]) were purchased from Precious Metals Online. Osmium(III) chloride hydrate (OsCl<sub>3</sub>·xH<sub>2</sub>O) was purchased from Strem Chemicals. Distilled water was purchased from Watsons Water.

**Characterization and instrumentation:** The metal nanoparticles and metal oxide nanocrystal samples were characterized by powder XRD, XPS, TEM, selected area electron diffrac-

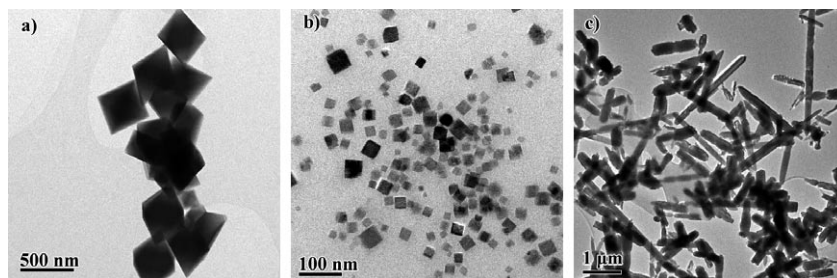


Figure 12. TEM images of a) Mn<sub>3</sub>O<sub>4</sub> nanooctahedrons, b) Co<sub>3</sub>O<sub>4</sub> nanocubes, and c) ZnO nanorods prepared in HEPES buffer (200 mM, pH 7.4) under hydrothermal conditions at 180 °C for 1 h.

tion (SAED), energy-dispersive X-ray microanalysis (EDX), SEM, and UV/Vis. The powder XRD measurement was performed on a Bruker D8 ADVANCE X-ray diffractometer with parallel  $\text{Cu}_{K\alpha}$  radiation ( $\lambda = 1.5406 \text{ \AA}$ ) and nickel filter. The scanning rate was  $0.005^\circ \text{ s}^{-1}$  in the  $2\theta$  range from  $30$  to  $90^\circ$  and the step size is  $0.05^\circ$ . Dry solid sample was placed on a glass slide for XRD measurement. XPS analysis was performed on a Physical Electronics Model 5600 with monochromatic  $\text{Al}_{K\alpha}$  as the X-ray source. TEM and SAED were done on Philips Tecnai G2 20 S-TWIN with an accelerating voltage of  $200 \text{ kV}$ . TEM images were taken by Gatan MultiScan Camera Model 794. The EDX analysis was performed on Oxford Instruments Inca with a scanning range from  $0$  to  $20 \text{ keV}$ . SEM images were taken on LEO 1530 FEG operating at  $5 \text{ kV}$ . The TEM sample was prepared by dropping a suspension of metal nanoparticles to the formvar-coated copper grids and then dried in a vacuum desiccator. The average particle size and monodispersity of the nanoparticles were measured against  $300$  nanoparticles by using DigitalMicrograph(TM) Demo 3.6.5 software. The SEM sample was prepared by putting solid sample onto silicon wafers, sticking onto the SEM specimen mounts. The pH of the buffer solution was measured by digital pH meter (HANNA Instruments), which was calibrated with pH standard buffer solutions (pH 7.010; Aldrich) in advance. UV/Vis absorption measurements were recorded on a Perkin-Elmer Lambda 900 UV/Vis spectrophotometer. The organic products were characterized by NMR spectroscopy ( $^1\text{H}$  and  $^{13}\text{C}$ ) and electron-impact mass spectrometry (EIMS).  $^1\text{H}$  and  $^{13}\text{C}$  NMR spectra were recorded on Bruker DPX-300, Avance400 or Bruker DPX-500 FTNMR spectrometers with chemical shifts (in ppm) relative to tetramethylsilane. Mass spectra were obtained on a Finnigan MAT 95 mass spectrometer.

**Preparation of HEPES buffer solution:** The HEPES buffer solution ( $200 \text{ mM}$ , pH 7.4) was prepared according to the literature report.<sup>[2c]</sup> In a typical experiment, HEPES ( $11.92 \text{ g}$ ,  $50 \text{ mmol}$ ) was first dissolved in deionized water ( $220 \text{ mL}$ ). The pH of this solution was about 5.4. Sodium hydroxide solution ( $1 \text{ M}$ ) was added slowly with vigorous stirring to adjust to pH 7.4. The buffer solution was diluted to  $250 \text{ mL}$  with deionized water to give HEPES buffer solution ( $200 \text{ mM}$ , pH 7.4). For a HEPES buffer solution with a concentration at  $5$  or  $50 \text{ mM}$  (pH 7.4), a desirable amount of HEPES was used and sodium hydroxide ( $0.1 \text{ M}$  or  $1 \text{ M}$ ) was used to adjust the pH of the buffer solution. The preparation of HEPES solution ( $200 \text{ mM}$ ) at pH 5.4 was simply done by dissolving HEPES ( $11.92 \text{ g}$ ,  $50 \text{ mmol}$ ) in deionized water ( $250 \text{ mL}$ ). The preparation of HEPES buffer solutions ( $200 \text{ mM}$ ) at pH 6.4, 8.4, and 9.4 were the same as above by using sodium hydroxide ( $1 \text{ M}$ ) for adjusting the pH of the solution.

**Synthesis of metal nanoparticles in HEPES buffer solution by using hydrothermal conditions:** In a typical procedure, metal salt ( $20 \mu\text{mol}$ ,  $5.2 \text{ mg}$   $\text{RuCl}_3 \cdot n\text{H}_2\text{O}$  for Ru nanoparticles,  $7.0 \text{ mg}$   $\text{OsCl}_3 \cdot n\text{H}_2\text{O}$  for Os nanoparticles,  $5.3 \text{ mg}$   $\text{RhCl}_3 \cdot n\text{H}_2\text{O}$  for Rh nanoparticles,  $7.0 \text{ mg}$   $\text{IrCl}_3 \cdot n\text{H}_2\text{O}$  for Ir nanoparticles,  $3.5 \text{ mg}$   $\text{PdCl}_2$  for Pd nanoparticles, and  $8.3 \text{ mg}$   $\text{K}_2\text{PtCl}_4$  for Pt nanoparticles) was dissolved in HEPES buffer solution ( $10 \text{ mL}$ ;  $200 \text{ mM}$ , pH 7.4). The mixture was stirred and ultrasonicated for  $15 \text{ min}$  to dissolve the metal salts. The mixture was transferred to the Teflon-lined stainless steel autoclave and underwent the hydrothermal synthesis at  $180^\circ\text{C}$  for  $1 \text{ h}$ . Suspensions of metal nanoparticles were subsequently produced. This synthetic protocol for metal nanoparticles was the same through the entire work unless otherwise specified (e.g. HEPES buffer of different concentration and pH, uses of EPPS, PIPES, and MES buffer).

Solid samples of metal nanoparticles for XRD analysis were obtained by the addition of a solvent mixture of acetone and ethanol (1:1) to induce the precipitation. The solid was collected by centrifugation and washed with a solvent mixture of water and ethanol (1:99) to remove the impurities and HEPES. The solid product was dried in a vacuum oven overnight. Calcination was done for certain samples to improve the crystallinity. The calcination was done at  $550^\circ\text{C}$  for  $6 \text{ h}$  under an argon atmosphere. The calcinated sample was kept under an argon atmosphere until the entire system was cooled to room temperature ( $25^\circ\text{C}$ ).

**Synthesis of metal nanoparticles in HEPES buffer solution by reflux conditions:** The metal nanoparticles were prepared in HEPES buffer solu-

tion under reflux conditions. In a typical procedure, metal salt ( $20 \mu\text{mol}$ ) was added to a refluxing HEPES buffer solution ( $10 \text{ mL}$ ,  $200 \text{ mM}$ , pH 7.4) at  $100^\circ\text{C}$ . The mixture was heated at  $100^\circ\text{C}$  for  $1 \text{ h}$ . A black precipitate was produced. This solid product was collected by centrifugation and washed three times with distilled water to remove impurities. The solid product was dried in a vacuum desiccator for characterization.

**Synthesis of graphite-supported metal nanoparticles:** Graphite ( $1 \text{ g}$ ) was added to the freshly prepared metal nanoparticles solution ( $0.1 \text{ mmol}$ ) and the mixture was stirred vigorously for  $1 \text{ day}$ . The MNPs/C catalyst was collected by centrifugation and washed three times with distilled water and absolute ethanol. The final product was oven-dried at  $75^\circ\text{C}$  for  $1 \text{ h}$  and stored in a desiccator for characterization.

**Synthesis of metal oxide nanocrystals in HEPES buffer solution by using hydrothermal conditions:** In a typical procedure, metal salt ( $20 \mu\text{mol}$ ,  $4.5 \text{ mg}$   $\text{MnSO}_4 \cdot 4\text{H}_2\text{O}$  for  $\text{Mn}_3\text{O}_4$  nanooctahedrons,  $4.8 \text{ mg}$   $\text{CoCl}_2 \cdot 6\text{H}_2\text{O}$  for  $\text{Co}_3\text{O}_4$  nanocubes,  $2.7 \text{ mg}$   $\text{ZnCl}_2$  for ZnO nanorods) was dissolved in HEPES buffer solution ( $10 \text{ mL}$ ;  $200 \text{ mM}$ , pH 7.4). The mixture was stirred and ultrasonicated for  $15 \text{ min}$  to dissolve the metal salts. The mixture was transferred to the Teflon-lined stainless steel autoclave and performed the hydrothermal process at  $180^\circ\text{C}$  for  $1 \text{ h}$ . After the hydrothermal process, the solid product was collected by centrifugation and washed three times with distilled water to remove impurities. The solid product was dried in a vacuum desiccator for characterization.

**Catalyst screening for aerobic oxidation of alcohol 1a:** Alcohols ( $0.4 \text{ mmol}$ ) and MNPs/C catalyst (metal:  $5 \text{ mol}\%$ ) were added to toluene ( $5 \text{ mL}$ ) in a glass tube connected with a condenser. The reaction flask was connected to an  $\text{O}_2$  gas supply ( $99.7\%$  min, Hong Kong Oxygen & Acetylene). The mixture was stirred and heated at  $110^\circ\text{C}$  for  $24 \text{ h}$ . By filtration against Celite, the MNPs/C catalyst was removed and the organic product was collected in the filtrate. Solvent was evaporated away under vacuum. The substrate conversion and product yield were determined by  $^1\text{H}$  NMR spectroscopy by using 1,1-diphenylethylene as the internal standard.

**Aerobic oxidation of alcohols:** Alcohols ( $0.4 \text{ mmol}$ ) and OsNPs/C catalyst (Os:  $5 \text{ mol}\%$ ) were added to toluene ( $5 \text{ mL}$ ) in a glass tube connected with a condenser. The reaction flask was connected to an  $\text{O}_2$  gas supply ( $99.7\%$  min, Hong Kong Oxygen & Acetylene). The mixture was stirred and heated at  $110^\circ\text{C}$  for a desired time. By filtration against Celite, the OsNPs/C catalyst was removed and the organic product was collected in the filtrate. Solvent was evaporated away under vacuum. The substrate conversion and product yield were determined by  $^1\text{H}$  NMR spectroscopy by using 1,1-diphenylethylene as the internal standard. Pure product was isolated by flash chromatography and identified by  $^1\text{H}$  and  $^{13}\text{C}$  NMR spectroscopy and EIMS.

## Acknowledgements

This work was supported by the Innovation and Technology Fund (ITS/189/08), University Development Fund, and the Hong Kong Research Grants Council (HKU 1/CRF/08 and CityU 2/06C). We thank Dr. Y. Liu for his helpful discussions and translation of the abstract from English to the traditional Chinese language. We offer our heartfelt thanks to F. Yu-Fee Chan and W.-S. Lee of the Electron Microscope Unit of the University of Hong Kong for their technical assistance.

- [1] Selected examples for the applications on electronic: a) M. L. Steigerwald, L. E. Brus, *Acc. Chem. Res.* **1990**, *23*, 183–188; b) L. D. Bozano, B. W. Kean, V. R. Deline, J. R. Salem, J. C. Scott, *Appl. Phys. Lett.* **2004**, *84*, 607–609; c) J. Ouyang, C. W. Chu, C. R. Szmanda, L. Ma, Y. Yang, *Nat. Mater.* **2004**, *3*, 918–922; d) C. H. Tu, D. L. Kwong, Y. S. Lai, *Appl. Phys. Lett.* **2006**, *89*, 252107–252109; e) S. Gamerith, A. Klug, H. Scheiber, U. Scherf, E. Moderegger, E. J. W. List, *Adv. Funct. Mater.* **2007**, *17*, 3111–3118; f) M.-H. So, V. A. L. Roy, Z.-X. Xu, S. S.-Y. Chui, M.-Y. Yuen, C.-M. Ho, C.-M. Che, *Chem. Asian J.* **2008**, *3*, 1968–1978; g) M.-Y. Yuen, V. A. L. Roy, W.

- Lu, S. C. F. Kui, G. S. M. Tong, M.-H. So, S. S.-Y. Chui, M. Muccini, J. Q. Ning, S. J. Xu, C.-M. Che, *Angew. Chem.* **2008**, *120*, 10043–10047; *Angew. Chem. Int. Ed.* **2008**, *47*, 9895–9899; h) T. Zheng, W. C. H. Choy, Y. Sun, *Adv. Funct. Mater.* **2009**, *19*, 2648–2653.
- [2] Selected examples for the applications on biological studies: a) T. Yamada, Y. Iwasaki, H. Tada, H. Iwabuki, M. K. Chuah, T. Vandendriessche, H. Fukuda, A. Kondo, M. Ueda, M. Seno, K. Tanizawa, S. Kuroda, *Nat. Biotechnol.* **2003**, *21*, 885–890; b) P. Alivisatos, *Nat. Biotechnol.* **2004**, *22*, 47–52; c) R. W.-Y. Sun, R. Chen, N. P.-Y. Chung, C.-M. Ho, C.-L. S. Lin, C.-M. Che, *Chem. Commun.* **2005**, 5059–5061; d) C. N. Lok, C.-M. Ho, R. Chen, Q.-Y. He, W.-Y. Yu, H. Sun, P. K.-H. Tam, J.-F. Chiu, C.-M. Che, *J. Proteome Res.* **2006**, *5*, 916–924; e) R. Chen, M.-H. So, J. Yang, F. Deng, C.-M. Che, H. Sun, *Chem. Commun.* **2006**, 2265–2267; f) Y. Iwasaki, M. Ueda, T. Yamada, A. Kondo, M. Seno, K. Tanizawa, S. Kuroda, M. Sakamoto, M. Kitajima, *Cancer Gene Ther.* **2007**, *14*, 74–81; g) C.-N. Lok, C.-M. Ho, R. Chen, Q.-Y. He, W.-Y. Yu, H. Sun, P. K.-H. Tam, J.-F. Chiu, C.-M. Che, *J. Biol. Inorg. Chem.* **2007**, *12*, 527–534; h) V. Sokolova, M. Epple, *Angew. Chem.* **2008**, *120*, 1402–1416; *Angew. Chem. Int. Ed.* **2008**, *47*, 1382–1395; i) N. Lewinski, V. Colvin, R. Drezek, *Small* **2008**, *4*, 26–49; j) M. A. Dobrovolskaia, A. K. Patri, J. Zheng, J. D. Clogston, N. Ayub, P. Aggarwal, B. W. Neun, J. B. Hall, S. E. McNeil, *Nanomed. Nanotechnol. Biol. Med.* **2009**, *5*, 106–117.
- [3] Selected examples for the applications on catalysis: a) A. Roucoux, J. Schulz, H. Patin, *Chem. Rev.* **2002**, *102*, 3757–3778; b) C.-M. Ho, W.-Y. Yu, C.-M. Che, *Angew. Chem.* **2004**, *116*, 3365–3369; *Angew. Chem. Int. Ed.* **2004**, *43*, 3303–3307; c) M. D. Hughes, Y.-J. Xu, P. Jenkins, P. McMorn, P. Landon, D. I. Enache, A. F. Carley, G. A. Attard, G. J. Hutchings, F. King, E. H. Stitt, P. Johnston, K. Griffin, C. J. Kiely, *Nature* **2005**, *437*, 1132–1135; d) D. Astruc, F. Lu, J. R. Aranzas, *Angew. Chem.* **2005**, *117*, 8062–8083; *Angew. Chem. Int. Ed.* **2005**, *44*, 7852–7872; e) D. I. Enache, J. K. Edwards, P. Landon, B. Solsona-Espriu, A. F. Carley, A. A. Herzing, M. Watanabe, C. J. Kiely, D. W. Knight, G. J. Hutchings, *Science* **2006**, *311*, 362–365; f) *Nanoparticles and catalysis* (Ed.: D. Astruc), Wiley-VCH, Weinheim, **2008**; g) Y. Zhu, C. N. Lee, R. A. Kemp, N. S. Hosmane, J. A. Maguire, *Chem. Asian J.* **2008**, *3*, 650–662; h) M. K.-W. Choi, W.-Y. Yu, M.-H. So, C.-Y. Zhou, Q.-H. Deng, C.-M. Che, *Chem. Asian J.* **2008**, *3*, 1256–1265; i) M.-H. So, Y. Liu, C.-M. Ho, C.-M. Che, *Chem. Asian J.* **2009**, *4*, 1551–1561.
- [4] a) *The chemistry of nanomaterials: synthesis, properties and applications, Vol. 2* (Eds.: C. N. R. Rao, A. Muller, A. K. Cheetham), Wiley-VCH, Weinheim, **2004**; b) *Nanomaterials chemistry: recent developments and new directions* (Eds.: C. N. R. Rao, A. Müller, A. K. Cheetham), Wiley-VCH, Weinheim, **2007**.
- [5] a) B. L. Cushing, V. L. Kolesnichenko, C. J. O'Connor, *Chem. Rev.* **2004**, *104*, 3893–3946; b) J. Park, J. Joo, S. G. Kwon, Y. Jang, T. Hyeon, *Angew. Chem.* **2007**, *119*, 4714–4745; *Angew. Chem. Int. Ed.* **2007**, *46*, 4630–4660; c) F. Fievet in *Fine Particles, Synthesis Characterization and Mechanism of Growth* (Ed.: T. Sugimoto), Marcel Dekker, New York, **2000**, pp. 460–496.
- [6] Fe nanoparticles: L.-M. Lacroix, S. Lachaize, A. Falqui, M. Respaud, B. Chaudret, *J. Am. Chem. Soc.* **2009**, *131*, 549–557; Co nanoparticles: J. Osuna, D. de Caro, C. Amiens, B. Chaudret, *J. Phys. Chem.* **1996**, *100*, 14571–14574; Ni nanoparticles: T. O. Ely, C. Amiens, B. Chaudret, E. Snoeck, M. Verelst, M. Respaud, J.-M. Broto, *Chem. Mater.* **1999**, *11*, 526–529; Cu nanoparticles: C. Barrière, G. Alcaraz, O. Margeat, P. Fau, J. B. Quoirin, C. Anceau, B. Chaudret, *J. Mater. Chem.* **2008**, *18*, 3084–3086; Ru nanoparticles: K. Pelzer, O. Vidoni, K. Philippot, B. Chaudret, V. Collière, *Adv. Funct. Mater.* **2003**, *13*, 118–126; Pd nanoparticles: S. Jansat, M. Gómez, K. Philippot, G. Muller, E. Guiu, C. Claver, S. Castillón, B. Chaudret, *J. Am. Chem. Soc.* **2004**, *126*, 1592–1593; Pt nanoparticles: F. Dassenoy, K. Philippot, T. O. Ely, C. Amiens, P. Lecante, E. Snoeck, A. Mosset, M.-J. Casanove, B. Chaudret, *New J. Chem.* **1998**, *22*, 703–712.
- [7] C. B. Murray, D. J. Norris, M. G. Bawendi, *J. Am. Chem. Soc.* **1993**, *115*, 8706–8715.
- [8] J. A. Dahl, B. L. S. Maddux, J. E. Hutchison, *Chem. Rev.* **2007**, *107*, 2228–2269.
- [9] a) P. Raveendran, J. Fu, S. L. Wallen, *J. Am. Chem. Soc.* **2003**, *125*, 13940–13941; b) P. Raveendran, J. Fu, S. L. Wallen, *Green Chem.* **2006**, *8*, 34–38.
- [10] a) Y. Xiong, I. Washio, J. Chen, H. Cai, Z.-Y. Li, Y. Xia, *Langmuir* **2006**, *22*, 8563–8570; b) I. Washio, Y. Xiong, Y. Yin, Y. Xia, *Adv. Mater.* **2006**, *18*, 1745–1749.
- [11] a) S. Tan, D. Pristinski, S. Sukhishvili, H. Du, *Proc. SPIE* **2005**, *6008*, art. no. 600808; b) S. Tan, M. Erol, A. Attygalle, H. Du, S. Sukhishvili, *Langmuir* **2007**, *23*, 9836–9843; c) S. Tan, M. Erol, S. Sukhishvili, H. Du, *Langmuir* **2008**, *24*, 4765–4771; d) Y. Han, S. Sukhishvili, H. Du, J. Cefaloni, B. Smolinski, *J. Nanosci. Nanotechnol.* **2008**, *8*, 5791–5800.
- [12] a) A. Habib, M. Tabata, *J. Inorg. Biochem.* **2004**, *98*, 1696–1702; b) A. Habib, M. Tabata, Y. G. Wu, *Bull. Chem. Soc. Jpn.* **2005**, *78*, 262–269; c) J. M. Slocik, M. O. Stone, R. R. Naik, *Small* **2005**, *1*, 1048–1052; d) R. Chen, PhD thesis, The University of Hong Kong (HK SAR), **2006**; e) B. K. Jena, C. R. Raj, *Langmuir* **2007**, *23*, 4064–4070; f) J. Xie, J. Y. Lee, D. I. C. Wang, *Chem. Mater.* **2007**, *19*, 2823–2830; g) J. Xie, Q. Zhang, J. Y. Lee, D. I. C. Wang, *ACS Nano* **2008**, *2*, 2473–2480; h) C.-L. Chen, P. Zhang, N. L. Rosi, *J. Am. Chem. Soc.* **2008**, *130*, 13555–13557; i) S. Diamanti, A. Elsen, R. Naik, R. Vaia, *J. Phys. Chem. C* **2009**, *113*, 9993–9997; j) T. Serizawa, Y. Hirai, M. Aizawa, *Langmuir* **2009**, *25*, 12229–12234.
- [13] a) A. L. Patterson, *Phys. Rev.* **1939**, *56*, 978–982; b) B. D. Cullity, S. R. Stock, *Elements of X-ray Diffraction*, Prentice Hall, Upper Saddle River, NJ, **2001**.
- [14] J. F. Moulder, W. F. Stickle, P. E. Sobol, K. D. Bomben in *Handbook of X-ray Photoelectron Spectroscopy* (Eds.: J. Chastain, R. C. King), Physical Electronic, Inc., Eden Prairie, **1995**.
- [15] a) S. Carrettin, P. Concepción, A. Corma, J. M. L. Nieto, V. F. Puentes, *Angew. Chem.* **2004**, *116*, 2592–2594; *Angew. Chem. Int. Ed.* **2004**, *43*, 2538–2540; b) A. Abad, P. Concepción, A. Corma, H. García, *Angew. Chem.* **2005**, *117*, 4134–4137; *Angew. Chem. Int. Ed.* **2005**, *44*, 4066–4069; c) P. Concepción, S. Carrettin, A. Corma, *Appl. Catal. A: Gen.* **2006**, *307*, 42–45.
- [16] Metal nanoparticle-catalyzed aerobic oxidation of alcohols: a) A. Corma, H. García, in *Nanoparticles and catalysis* (Ed.: D. Astruc), Wiley-VCH, Weinheim, **2008**, pp. 389–426 and references therein; b) C. D. Pina, E. Falletta, M. Rossi in *Nanoparticles and catalysis* (Ed.: D. Astruc), Wiley-VCH, Weinheim, **2008**, pp. 427–455 and references therein.

Received: January 25, 2010